# ISOPHOT*APERTURE PROFILES AND BACKGROUND MEASUREMENTS

**T.G. Müller**
ISO Data Centre, ESA Astrophysics Division, Villafranca del Castillo, P.O. Box 50727, 28080 Madrid, Spain

## ABSTRACT

Multi-aperture measurements with ISOPHOT display in some cases an abnormal behaviour. The measured *signal to aperture area* ratio on uniform sky backgrounds is not constant. This observing template has therefore not yet been scientifically validated.

Here aperture profile measurements are presented, which show that a point source placed at various positions within the aperture can produce quite different signals. This means that the aperture profiles are not flat as one would expect. Additionally the position dependent sensitivity changes with filter. Although some of the aperture profiles show strong gradients they alone cannot explain the peculiar behaviour of the aperture sequences on the sky background. Only by shifting the aperture centres additionally a few *arcsec* relative to each other the modeling of the measured signals is possible.
The results have implications for sky measurements in so-called nonstandard apertures, since the measured background fluxes do not scale with the corresponding aperture area. Due to the gradients in the aperture profiles, observations of extended structures depend on the role-angle of the satellite. And last, but not least, photometry of point sources are affected if the objects are a few *arcsec* off-centre.

All results presented here are based on pure sky observations. No internal FCS[1] calibration measurements are considered to avoid additional complications.

Key words: ISO; Infrared Astronomy; Multi-Aperture Photometry; Aperture Scans; Aperture Profiles; Extended Sources.

## 1. INTRODUCTION

At first sight, observing a homogeneous sky background with a set of different apertures of ISOPHOT seems to be a simple measurement and the measured flux should scale linearly with the aperture area. This was unfortunately not the case and several investigations were necessary to understand the observations (Walker et al. 1996; Heinrichsen 1997; Herbstmeier 1998a; Radovich 1998; Müller 1998). In the ISOPHOT PHT04 AOT[2] it was possible to select a filter between $3.3\mu m$ and $100\mu m$, in combination with a set of circular apertures, ranging from 5" to 180" diameter (Klaas et al. 1994; see Figure 1).

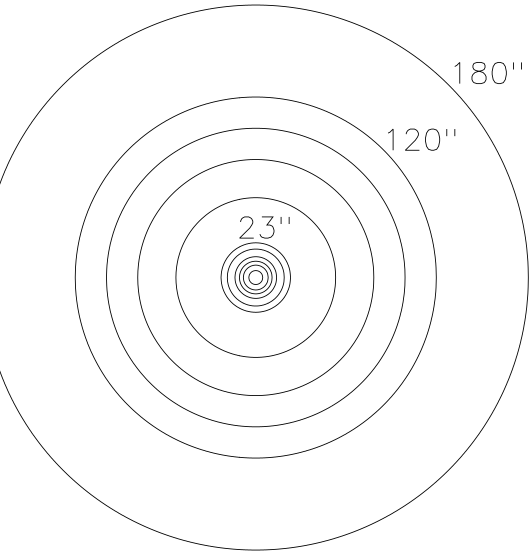


*Figure 1. Relative sizes of ISOPHOT circular apertures, ranging from 5" to 180",for the detectors P1, P2 and P3.*

By switching from the smallest aperture to the biggest one, the aperture area changes more than 3 orders of magnitude, which corresponds to a signal increase by 3 orders of magnitude on a flat extended source (i.e. zodiacal light, cirrus background) within one measurement sequence. Transient and non-linearity effects play therefore a major role in the analysis of the observations. And only recently it became possible to include detector non-linearities (Schulz et al. 1999b). The PHT04 AOT included also one internal FCS calibration measurement, performed in the largest selected aperture (usually the

*ISO is an ESA project with instruments funded by ESA Member States (especially the PI countries: France, Germany, the Netherlands and the United Kingdom) and with the participation of ISAS and NASA.
[1] Fine Calibration Source
[2] Astronomical Observation Template

180” aperture). But the general photometric calibration is based on measurements in the so-called “standard” aperture (see Schulz et al. 1999a). To avoid complications from FCS measurements in different apertures, only sky observations have been considered and the analysis is done in a relative way.

In the following sections aperture scans and PHT04 measurements on bright background positions are presented and the data reduction methods are described (Sections 2., 3., 4.). In Section 5. the results are summarized and later on discussed (Section 6.).

## 2. OBSERVATIONS AND DATA REDUCTION

### 2.1. APERTURE SCANS AND PHT04 BACKGROUND OBSERVATIONS

Aperture profile cross scans at 7.3, 12.0 and 16 $\mu m$ have been used in parallel with PHT04 sequences in order to assess the radial response of the apertures. These calibration measurements include raster maps (PHT03) on a point source, using 180” or 52” aperture and sparse maps (PHT17, PHT18, PHT19) to map the edges of these apertures (see Figure 2). Standard apertures for ISOPHOT are 23” ($3.3 - 7.7\,\mu m$), 52” ($10 - 16\,\mu m$), 79” ($20 - 25\,\mu m$) and 180” ($60 - 100\,\mu m$).

During raster maps the telescope was pointing along the satellite y- and z-axis (forward & backward scan) to place the star at different positions within the apertures. Sparse maps repeated those parts of the scans covering the edges of the aperture.

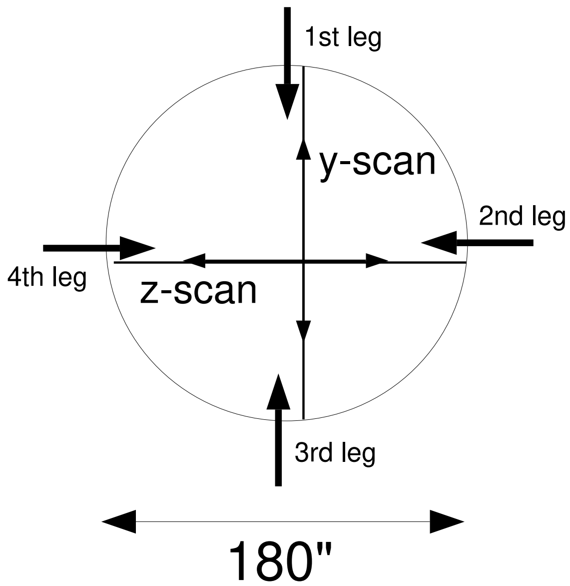


*Figure 2. Aperture profile scans (forward and backward scans, performed as raster maps) and sparse maps at the edges of the* 180” *aperture, using a bright standard star.*

All observations are summarized in Table 1, part I.

In PHT04 sequences the source is centered and the different apertures are used sequentially going from small to big ones, with a FCS measurement in the biggest aperture at the end of the sequence. Calibration measurements performed with the AOT PHT04 (Multi-aperture Photometry) on selected background positions are given in part II of Table 1.

### 2.2. ISOPHOT DATA REDUCTION

All PHT-data have been processed with ISOPHOT Interactive Analysis (PIA[3]) V8.0 (Gabriel et al. 1997). The standard data reduction from ERD to SCP level included ramp linearization and ramp deglitching on ERD level, reset interval correction, deglitching, dark current subtraction and signal linearization on SRD level and drift recognition when processing to SCP level. One critical point in the procedure is the signal linearization which accounts for a nonlinear detector response at different flux levels (Schulz et al. 1999b and Huth & Schulz 1998). The influence of signal linearization on absolute level is shown in Figure 3 for a bright background.

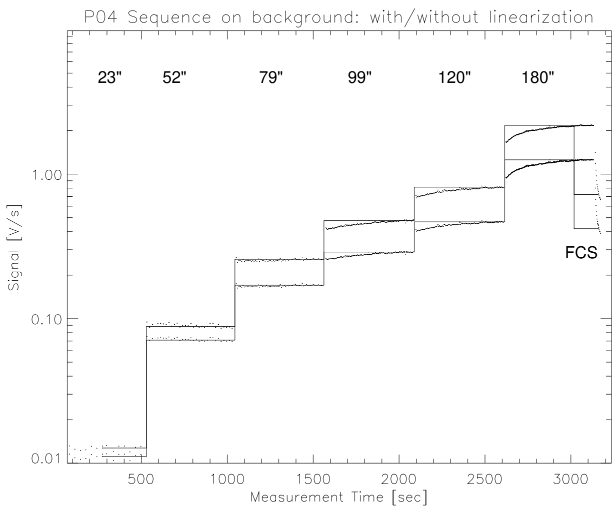


*Figure 3. Effect of signal linearization on a bright background position: Upper sequence with and lower sequence without signal linearization. The SRD data are given as dots, the SCP results in histogram mode.*

All measured physical aperture sizes (ZEISS 1990a) and the projected diameter on the sky are given in Table 2.

## 3. APERTURE PROFILES FROM CROSS SCANS

Performing an aperture sequence on a non-structured background position should result in signals which increase linearly with the aperture area. But measurements of the aperture footprints (see Figures 4,

[3]PIA is a joint development by the ESA Astrophysics Division and the ISOPHOT consortium.

*Table 1. List of all Observations.*

I. Aperture scans

| TDT | PROPID | DATE | AOTs | Det | Fil | Aper | Source/Observation |
|---|---|---|---|---|---|---|---|
| 79701201f | P1BEAM01 | 20-Jan-1998 | PHT17/PHT19 | P1 | 12.0 | 180 | HR0440 off/on position |
| 79701303f | P1BEAM01 | 20-Jan-1998 | PHT03 | P1 | 12.0 | 180 | HR0440 Y-scan/Z-scan |
| 79701405ff | P1BEAM01 | 20-Jan-1998 | PHT17/18/19 | P1 | 12.0 | 180 | HR0440 sparse map leg1 |
| 79701511ff | P1BEAM01 | 20-Jan-1998 | PHT17/18/19 | P1 | 12.0 | 180 | HR0440 sparse map leg2 |
| 79701617ff | P1BEAM01 | 20-Jan-1998 | PHT17/18/19 | P1 | 12.0 | 180 | HR0440 sparse map leg2 |
| 79701723ff | P1BEAM01 | 20-Jan-1998 | PHT17/18/19 | P1 | 12.0 | 180 | HR0440 sparse map leg2 |
| 84201701f | P1BEAM02 | 06-Mar-1998 | PHT17/PHT19 | P1 | 7.3 | 180 | HR1396 off/on position |
| 84201703f | P1BEAM02 | 06-Mar-1998 | PHT03 | P1 | 7.3 | 180 | HR1396 Y-scan/Z-scan |
| 84201705ff | P1BEAM02 | 06-Mar-1998 | PHT17/18/19 | P1 | 7.3 | 180 | HR1396 sparse map leg1 |
| 84201711ff | P1BEAM02 | 06-Mar-1998 | PHT17/18/19 | P1 | 7.3 | 180 | HR1396 sparse map leg2 |
| 84201717ff | P1BEAM02 | 06-Mar-1998 | PHT17/18/19 | P1 | 7.3 | 180 | HR1396 sparse map leg3 |
| 84201723ff | P1BEAM02 | 06-Mar-1998 | PHT17/18/19 | P1 | 7.3 | 180 | HR1396 sparse map leg4 |
| 86705301f | P1BEAM05 | 31-Mar-1998 | PHT17/PHT19 | P1 | 16.0 | 180 | HR7310 off/on position |
| 86705303f | P1BEAM05 | 31-Mar-1998 | PHT03 | P1 | 16.0 | 180 | HR7310 Y-scan/Z-scan |
| 86705305ff | P1BEAM05 | 31-Mar-1998 | PHT17/18/19 | P1 | 16.0 | 180 | HR7310 sparse map leg1 |
| 86705311ff | P1BEAM05 | 31-Mar-1998 | PHT17/18/19 | P1 | 16.0 | 180 | HR7310 sparse map leg2 |
| 86705317ff | P1BEAM05 | 31-Mar-1998 | PHT17/18/19 | P1 | 16.0 | 180 | HR7310 sparse map leg3 |
| 86705323ff | P1BEAM05 | 31-Mar-1998 | PHT17/18/19 | P1 | 16.0 | 180 | HR7310 sparse map leg4 |
| 86706501f | P1BEAM06 | 31-Mar-1998 | PHT17/PHT19 | P1 | 12.0 | 52 | HR1464 off/on position |
| 86706503f | P1BEAM06 | 31-Mar-1998 | PHT03 | P1 | 12.0 | 52 | HR1464 Y-scan/Z-scan |
| 86706505ff | P1BEAM06 | 31-Mar-1998 | PHT17/18/19 | P1 | 12.0 | 52 | HR1464 sparse map leg1 |
| 86706511ff | P1BEAM06 | 31-Mar-1998 | PHT17/18/19 | P1 | 12.0 | 52 | HR1464 sparse map leg2 |
| 86706517ff | P1BEAM06 | 31-Mar-1998 | PHT17/18/19 | P1 | 12.0 | 52 | HR1464 sparse map leg3 |
| 86706523ff | P1BEAM06 | 31-Mar-1998 | PHT17/18/19 | P1 | 12.0 | 52 | HR1464 sparse map leg4 |

II. Aperture sequences on background positions

| TDT | PROPID | DATE | AOT | Det | Fil | Apertures ["] | Source |
|---|---|---|---|---|---|---|---|
| 71301001 | 52512003 | 28-Oct-1997 | PHT04 | P1 | 7.3 | 23,52,79,99,120,180 | Bright region |
| 87500103 | P04PSF02 | 08-Apr-1998 | PHT04 | P1 | 7.3 | 13.8,18,23,52,79,99,120,180 | Bgr (HR7127) |
| 71301102 | 52512003 | 28-Oct-1997 | PHT04 | P1 | 12.0 | 10,13.8,18,23,52 | Bright region |
| 71301103 | 52512003 | 28-Oct-1997 | PHT04 | P1 | 12.0 | 52,79,99,120,180 | Bright region |
| 56600502 | 52512001 | 04-Jun-1997 | PHT04 | P1 | 16.0 | 52,79,99,120,180 | Bright region |
| 60802402 | 52512002 | 16-Jul-1997 | PHT04 | P1 | 16.0 | 52,79,99,120,180 | Bright region |
| 80500803 | P04PSF01 | 28-Jan-1998 | PHT04 | P2 | 20.0 | 10,13.8,18,23,52,79,99,120,180 | Bgr (HR617) |
| 71301204 | 52512003 | 28-Oct-1997 | PHT04 | P2 | 25.0 | 79,99,120,180 | Bright region |
| 72002401 | 5412P204 | 05-Nov-1997 | PHT04 | P2 | 25.0 | 23,52,79,99,120,180 | Bgr (HR7980) |
| 80500701 | P04PSF01 | 28-Jan-1998 | PHT04 | P2 | 25.0 | 23,52,79,99,120,180 | Bgr (HR617) |
| 71302105 | 52512003 | 28-Oct-1997 | PHT04 | P3 | 60.0 | 79,99,120,180 | Bright region |
| 79600205 | P04PSF01 | 19-Jan-1998 | PHT04 | P3 | 60.0 | 23,52,79,99,120,180 | Bgr (HR6705) |
| 80501507 | P04PSF01 | 28-Jan-1998 | PHT04 | P3 | 60.0 | 18,23,52,79,99,120,180 | Bgr (HR337) |
| 81500709 | P04PSF01 | 07-Feb-1998 | PHT04 | P3 | 60.0 | 10,13.8,18,23,52,79,99,120,180 | Bgr (HR1457) |

5, 6 and 7) show that the aperture profile is not flat: placing a point source at different positions within the aperture resulted in significantly different signals depending on the position within the aperture. The errorbars reflect the differences between forward and backward scan. Additional measurements at the edges of the 180" aperture are plotted with $*$-symbols (see also Figure 2. These profile measurements have been reduced exactly in the same way as all PHT04 sequences, including also the signal linearization correction.

From the measured aperture scans it is possible to produce 3-dimensional profiles. All scans have been background subtracted and normalized to 1.0 at the central position. The background was determined at both outer points of the scans and linearly interpolated in between.

The interpolation in the 4 sections between the scans was done with a spline fit through all measured values at the same radial distance (see Figure 8). Figure 9 shows the results at 12.0 $\mu m$ for the 180" and 52" apertures, Figure 10 shows the results for 7.3 $\mu m$ and 16.0 $\mu m$, for the 180" aperture.

Although the profiles show strong asymmetries, the ratio of the two integrated profiles at 12.0 $\mu m$ in Figure 9 is 11.79, which is, within the given uncertainties, the same as the ratio of the two aperture areas (11.65). Performing an artificial aperture sequence on the constructed profiles, by cutting out the corresponding volumes from Figure 9 (a), confirms also the volumes increase proportional to the aperture areas. Accepting 5 % uncertainty, the *volume over aperture area*-ratio is constant for all apertures. Of course, this assumes that all apertures are mounted concen-

*Table 2. ISOPHOT circular apertures, measured physical sizes and diameters on the sky (ZEISS 1990a).*

| Name | Area [$mm^2$] | Diameter [”] |
|---|---|---|
| 5 | 0.0314 | 4.6 |
| 7P6 | 0.1001 | 8.2 |
| 10 | 0.1735 | 10.8 |
| 13P8 | 0.2827 | 13.7 |
| 18 | 0.5281 | 18.8 |
| 23 | 0.7854 | 22.9 |
| 52 | 4.1548 | 52.7 |
| 79 | 9.0792 | 77.9 |
| 99 | 14.5220 | 98.5 |
| 120 | 21.2372 | 119.2 |
| 180 | 48.3982 | 179.9 |

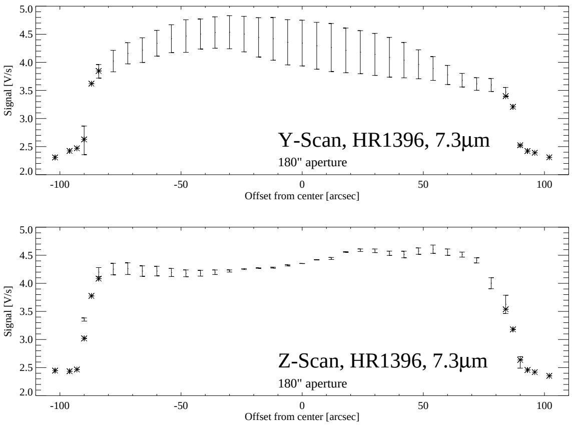


*Figure 4. Aperture profile scans at 7.3 µm, 180” aperture on the star HR 1396. Error bars indicate the signal reproducibility in the forward and backward scans.*

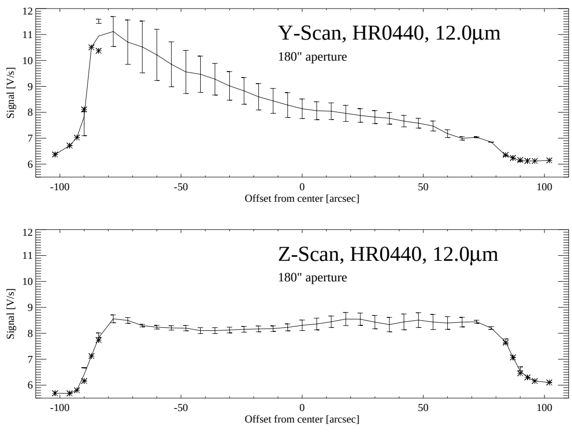


*Figure 5. Aperture profile scans at 12.0 µm, 180” aperture on the star HR 0440.*

trically and, for example the 52” aperture sees really the central 52” of the 180” aperture and not an off-center shifted area.

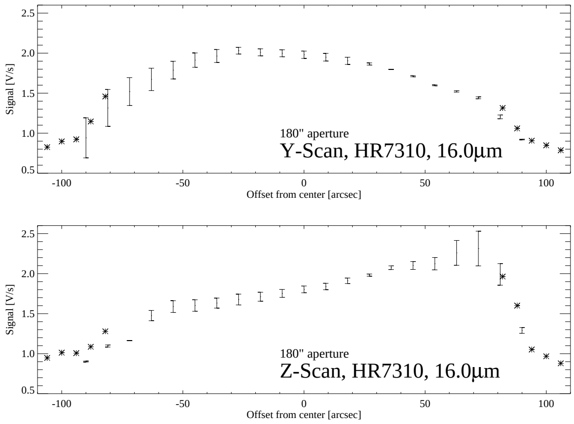


*Figure 6. Aperture profile scans at 16.0 µm, 180” aperture.*

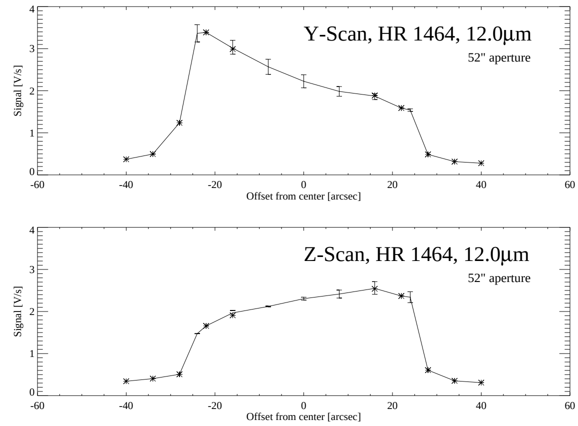


*Figure 7. Aperture profile scans at 12.0 µm, 52” aperture.*

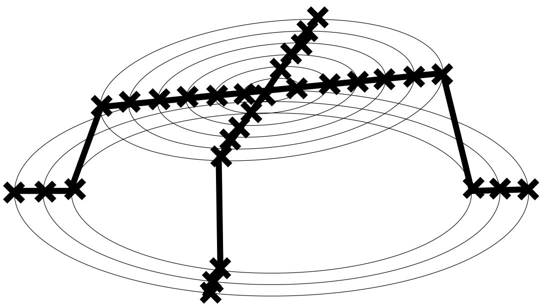

*Figure 8. From cross scans to 3 dimensional aperture profiles. The interpolation was done with a spline fit through all measured values at the same radial distance.*

The reason for the asymmetric aperture profiles is not known. One explanation could be that the projection of the aperture, located in the focal plane,

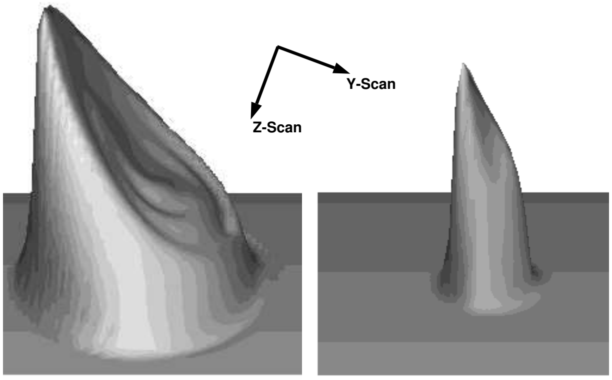


*Figure 9. Constructed 3-D aperture profile at* 12.0 $\mu m$. *(a) for the* 180" *aperture, (b) for the* 52" *aperture. Both profiles are normalized to 1.0 in the center.*

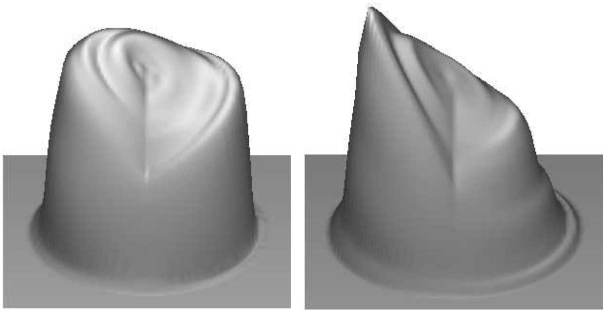

*Figure 10. Constructed 3-D aperture profile at (a)* 7.3 $\mu m$, 180" *aperture, (b) at* 16.0 $\mu m$, 180" *aperture. Both profiles are normalized to 1.0 in the center.*

onto the detector is not perfect. The projection is done via a Fabry lens (P1 detector) or via elliptical Fabry mirrors (P2 and P3 detectors). The detectors are sitting in cavities and internal reflections might cause different responses of the detector, depending on the position of a source within the aperture. For a detailed description of the detector-cavity configuration see also Battelle (1993), a precise overview over the optical design for the P-detectors can be found in ZEISS (1988).

## 4. MULTI-APERTURE SEQUENCES ON BRIGHT BACKGROUND POSITIONS

Analysing PHT04 aperture sequences on the sky (bright background positions: zodiacal light and/or cirrus) gives a completely different picture. The measured *signal to aperture area* ratio is not constant anymore. Figure 11 shows the measured signals divided by the aperture area and normalized to the 180" aperture for the 3 filters with aperture scans. The measured signals themselves are well determined due to long integration times. Examples for signals measured with the P1 detector are shown in Figure 13.

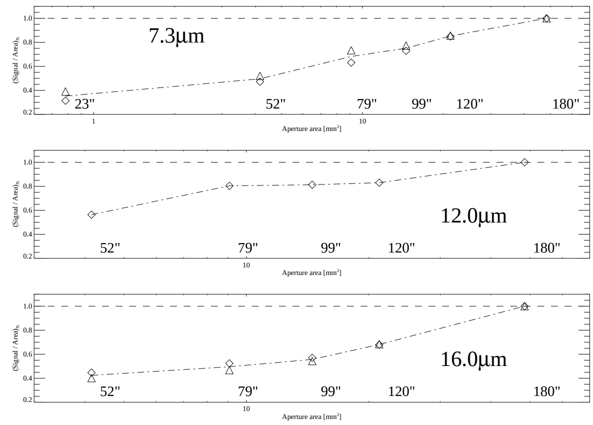


*Figure 11. PHT04 Sequences on bright background positions with the P1 detector for filters with aperture scans. Measured signals are divided by the aperture area and normalized to the* 180"*-aperture for the* 7.3 $\mu m$, 12.0 $\mu m$ *and* 16.0 $\mu m$ *filters.*

Figure 12 shows the same analysis for the P2 and P3 detectors per filter. The P3, 60 $\mu m$ plot shows a different behaviour. This might be the influence of diffraction (see also Figure 2 in Müller 1999).

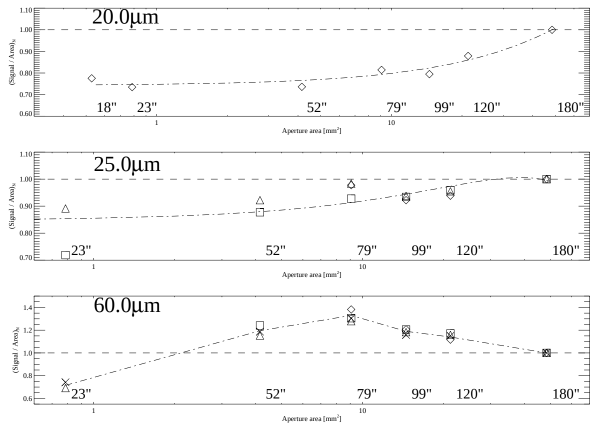


*Figure 12. PHT04 Sequences on bright background positions with the P2- and the P3-detectors. Measured signals are divided by the aperture area and normalized to the* 180"*-aperture.*

The smaller apertures see significantly less flux then one would expect from flat aperture profiles. Even the roof-shaped profiles (Figure 9 and Figure 10) cannot explain signal losses up to 50% (if all apertures are centered on the same position). The resulting values are summarized in Table 3.

Herbstmeier (1998b) and Walker & Herbstmeier (1997) investigated P2 and P3 beam profiles in comparison with models. In case of P3 they reported slight asymmetric profiles, which they attributed to "artefacts of the positioning or sampling". For P2 footprint measurements at 25 $\mu m$ in the 23", 79" and the 20" $\times$ 32" have been analysed. The measured asymmetry of the Z-cuts and the double peaks in the

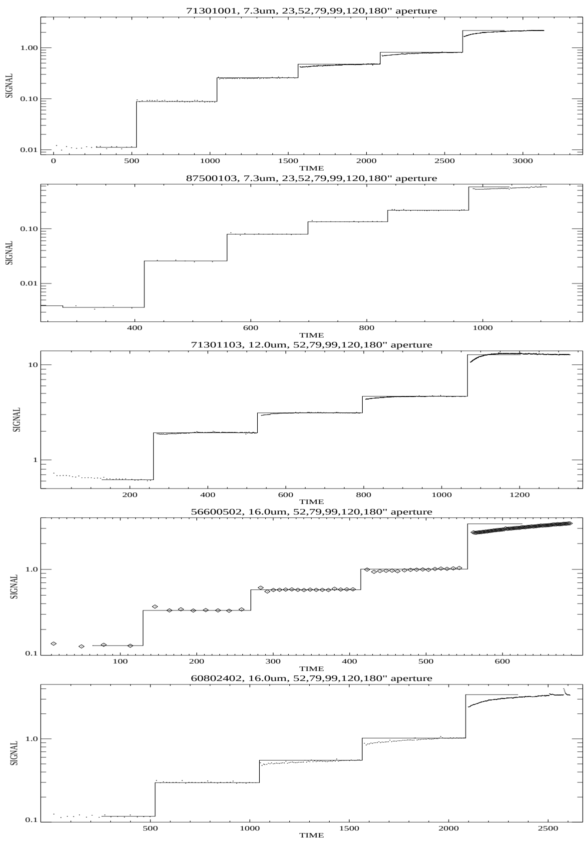


*Figure 13. Aperture signal sequences on bright background positions with the P1-detector.*

*Table 3. Measured signal per aperture area relative to the* $180''$ *aperture.*

| Filter | $23''$ | $52''$ | $79''$ | $99''$ | $120''$ | $180''$ |
|---|---|---|---|---|---|---|
| P_7.3 | 0.35 | 0.50 | 0.68 | 0.75 | 0.85 | 1.00 |
| P_11.5 | | 0.56 | 0.80 | 0.81 | 0.83 | 1.00 |
| P_16.0 | | 0.42 | 0.50 | 0.56 | 0.68 | 1.00 |
| P_20 | 0.75 | 0.77 | 0.80 | 0.83 | 0.86 | 1.00 |
| P_25 | 0.80 | 0.90 | 0.95 | 0.93 | 0.96 | 1.00 |
| P_60 | 0.72 | 1.20 | 1.33 | 1.19 | 1.14 | 1.00 |

Y-cuts ±20" distant from the central point could not be reproduced by the model. Herbstmeier (1998b) finds for the 79" aperture at $25\,\mu m$ between modeled and measured footprints an offset of 7" in negative Z-direction. He concluded that these features are due to the internal light path of the ISOPHOT instrument.

## 5. RESULTS AND DISCUSSION

Comparisons between the cross scans in Figures 4, 5, 6, 7 and the aperture sequences in Figure 11 are not easy to make due to the limited information coming from the cross scans. The behaviour in the remaining sections of the aperture is not known. Since drift stabilized aperture cross scans were only done at $7.3\,\mu m$ (180"), $12.0\,\mu m$ (52", 180") and at $16.0\,\mu m$ (180"), no good quality information about the other filters is available. Additional two-dimensional aperture scans have been performed, but they are seriously affected by drifts (Klaas, priv. communication).

The aperture cross scans revealed strong sensitivity variations at different positions within the apertures, but could not explain observations of sky background positions. From ground-based laboratory measurements it is known that the apertures are not perfectly aligned (ZEISS 1990b) and that the optical alignment changed during vibration tests (ZEISS 1990c and ZEISS 1992). The comparison in Section 3. between the integrated flux in the 180" and the 52" aperture assumed a perfect alignment of both apertures and a normalization to 1.0 at the center. But a slight shift of the 52" aperture towards the positive Y-axis would strongly decrease the integrated flux in relation to the 180" integrated flux (in Section 3. both profiles have been normalized to 1.0 at the center). Unfortunately no cross scans with the same source in different apertures exist (here: HR 0440 measured at $12\,\mu m$, 180" and HR 1464 at $12\,\mu m$, 52"). Therefore the comparison between the integrated fluxes from different apertures depends strongly on the way the normalization of the scans is done. Assuming only a 52"-center to 180"-centre offset of 8" produces already more than 30% signal loss (or gain) relative to the corresponding aperture area, depending on the offset direction. ZEISS (1990b) reports offsets larger than the tolerance of $0.08\,mm$ (approx. 2") for a few fieldstops. These offsets changed during the vibration tests (ZEISS 1990c and 1992). The maximal offset found by ZEISS was approximately 4". Assuming the worst case of 2 apertures, shifted both by 4" but in opposite directions, would be sufficient to explain the findings.

Due to the limited information about the real aperture profiles, this gain or loss in flux could be even bigger, depending on the real profile of the apertures. From observations alone it is not possible to determine the real center-to-center offsets, but offset of several arcsecs are easily possible.

## 6. CONCLUSION

From the analysis of the presented aperture calibration measurements the following results have been found:

- Direct measurements clearly show that the P1-aperture profiles are asymmetric. From aperture sequences on bright background positions it became clear that P2 and P3 aperture profiles also show peculiar behaviour. The P2 profile analysis by Herbstmeier (1998b) confirms these findings. Probably all aperture profiles are asymmetric and roof-shaped.
- The asymmetry in the roof-shaped profiles alone cannot explain the *signal per area* loss in smaller apertures relative to the 180" aperture.
- It seems that the PHT04 peculiar behaviour, with varying *signal per aperture area*, can be ex-

plained by the asymmetric profiles in combination with small center-to-center offsets (which have already been seen in laboratory measurements).

This leads to the following conclusions and implications for the data reduction:

a) Several observers used the 180" aperture to determine the background flux, while the scientific object was measured in the standard aperture. Here the deviations in the aperture behaviour are quite important and have to be taken into account. One possibility would be to scale the measured background signal with the values given in Table 3 to the aperture in which the target has been observed and subtract it from the target signal. The FCS calibration of *on-source minus scaled background* can then be done afterwards.

b) The analysis of extended sources and the reliability of maps are strongly influenced by the roof shaped aperture profiles. The measured flux of a bright off-center structure depends on the part of the aperture which sees this structure. With changing role-angle of the satellite the flux of the extended structure will also change.

c) In cases where a point-source is several *arcsec* off-center, the aperture photometry will not be reliable any more. Repeated measurements of the same point source can lead to a large scatter in the photometry due to pointing uncertainties in combination with the position dependent sensitivity within the apertures.

d) For the scientific analysis of PHT04 Multi-aperture photometry the results from background sequences can be used with the following steps:

1: Determination of the sky background from dedicated background measurements or from the analysis of the two largest apertures.

2: Scaling the background contribution in individual apertures with the results from Section 4.. For example: At $16.0\,\mu m$ the 79" aperture sees only 50% of the background signal as compared to the 180" aperture.

3: Subtracting the scaled background (or adding it to the modeled extended source) for each individual aperture.

The applicability of the method for the PHT04 multi-aperture photometry will be shown in a forthcoming Paper II by Müller (1999).

## Acknowledgments

Part of this work was done at the Max-Planck-Institut für Astronomie (MPIA) in Heidelberg. I thank Carlos Gabriel, Ulrich Klaas, Rene Laureijs and Bernhard Schulz for many discussions. Especially the proof reading and comments of Ulrich Klaas were very helpful and improved the paper significantly. Ulrich Grözinger provided the technical documentation of ISOPHOT.

I also would like to thank Bernhard Schulz for presenting these results at the workshop "ISO beyond point sources: Studies of extended infrared emission".

## REFERENCES

Battelle 1993, "ISOPHOT Abschlußbericht", RP-PHT-4760BF/93, pages 88/89, 30.09.1993

Gabriel, C., Schulz, B., Acosta–Pulido, J. A. *et al.* 1997, Proc. of ADASS VI, 112

Heinrichsen I., Dec. 1997, ISOPHOT Internal Report: "Report on First Results of P04 Multi-aperture Photometry Calibration Programme Pilot Observation"

Herbstmeier U. 1998a, ISOPHOT Footprints and Near-Field Straylight, several ISOPHOT internal reports, 1998

Herbstmeier U. 1998a, "P2 - Comparison between modelled and measured footprints - the derived parameters", ISOPHOT internal report, 1998

Huth S. and Schulz B., May 1998, ISOPHOT Internal Report: "Investigation of the flux dependency of the detector responsivity for the ISOPHOT P- and C-detectors"

Klaas U., Krüger H., Heinrichsen, I. *et al.* 1994, ISOPHOT Observer's Manual, ESA/ESTEC, Noordwijk, Version 3.1

Müller T.G., 1998, "Analysis of Multi-aperture Photometry (including EXTBEAM, PHT04PSF, photometry in nonstandard apertures)", 08-July-1998, ISOPHOT internal report

Müller T.G., 1999, same proceedings, "ISOPHOT APERTURE SEQUENCES ON POINT- AND EXTENDED SOURCES"

Radovich M., "Analysis of Photometry in Non-Standard Apertures", ISOPHOT internal report, 1998

Schulz B., Huth S., Kinkel U., Lemke D., Acosta–Pulido J.A, Braun M., Castañeda, Cornwall L., Gabriel C., Heinrichsen I., Herbstmeier U., Klaas U., Laureijs R.J. and Müller T.G., 1999a, "ISOPHOT - PHOTOMETRIC CALIBRATION OF POINT SOURCES", ISO Conference Proceedings, ESA SP-427, 1999

Schulz B., 1999b, "Linearisation of ISOPHOT-P and C detector signals in OLP8", ISOPHOT internal report, in preparation

Walker H., Heinrichsen I., Laureijs R.J. and Klaas U., PHT04 AOT Commissioning Report, ISOPHOT internal report, 1996

Walker H. and Herbstmeier U., "P3 Beam Profiles and Straylight", ISOPHOT internal report, 1997

ZEISS 1988, Technical Note: "Detailed Design Review", CZ-PHT-TN-023, 18.11.88

ZEISS 1990a, Non Conformance Report: "Stop-diameter for Wheel 2 (FM)", CZ-NCR-222201/167, 06.11.1990

ZEISS 1990b, Non Conformance Report: "Optical alignment of stop", CZ-NCR 222202/163, 26.10.90

ZEISS 1990c, Non Conformance Report: "Optical Alignment after Vibration (CHW-II-FM)", CZ-NCR-222202/186, 03.12.90

ZEISS 1992, Non Conformance Report: “Optical Alignment after Vibration (CHW-II-FM)”, CZ-NCR-222202/186, reopened 17.09.1992